The 9th European Congress on Computational Methods in Applied Sciences and Engineering
ECCOMAS Congress 2024
3–7 June 2024, Lisboa, Portugal

IMPLICIT LES VIA SPECTRAL/HP CG METHODS: RATIONALE AND COMPARISON TO OTHER LES/ILES

DANIEL GARCIA-RIBEIRO[1], AUGUSTO H. P. ZANCA[1], VINÍCIUS MALATESTA[1], RODRIGO C. MOURA[1] AND SPENCER J. SHERWIN[1]

[1] Instituto Tecnológico de Aeronáutica
São José dos Campos, Brazil

[2] Imperial College London
London, United Kingdom

Key words: Spectral Element Methods, CG, iLES, LES, GJP, High-order methods

Summary. Spectral element methods (SEM) are receiving increased attention over recent years given their capability to yield LES-type results without turbulence models (implicit LES – iLES). There is, though, a lack of fundamental studies on the suitability of continuous Galerkin (CG) methods, as most studies have focused on discontinuous SEM. This work aims to investigate solution quality and numerical robustness of CG-iLES by discussing simulations of the Taylor-Green Vortex and of spatially-developing turbulent channel flows. The performance of a recently developed stabilization technique (GJP) receives special attention. We show that CG-iLES with GJP can outperform traditional LES and be competitive alongside discontinuous SEM iLES.

1 INTRODUCTION

Fluid mechanics if a field that encompasses many engineering applications. Many of them require the use of computational methods for their development, for instance aircraft and wind turbines. There are many types of computational analyses, usually they are linked to the desired level of fidelity. In fluid mechanics problems, the fidelity is related with turbulence, that is a state of fluids motion characterized by unsteadiness, irregularity and chaos. The velocity field of a turbulent flow will present a mean component and considerable fluctuations around that mean value, exhibiting a large range of time and length scales [1].

A computational analysis is helpful to model and solve turbulent flows, but it can often become impractical to be performed if the direct numerical approach (DNS) of solving the governing equations is employed due to the amount of information contained in a turbulent flow field. On the other hand, the Large Eddy Simulation (LES) turbulence approach applies a filter on the Navier-Stokes (NS) equations to directly solve only the large-scales of the flow field and it models the influence of the small-scales with a sub-grid scale (SGS) model. Here, we deal with the implict LES approach, or also called under-resolved DNS, where the dissipation effects of the smallest scales are not modeled, but relied on the numerical method's intrinsic dissipation.

As for the numerical methods, they are employed to obtain a discretized version of the NS equations and then a solution. Here, we apply the Spectral/hp Element Methods (SEM) as these high-order methods have been presenting interesting properties as suitable numerical dissipation and good accuracy [2, 3, 4]. Among the SEM, we can cite the Continuous Galerkin

(CG) and Discontinuous Galerkin (DG) methods. These spectral methods are based on the idea to represent the numerical solution using high-order polynomial bases inside each mesh element. The DG scheme possesses solution discontinuity among mesh elements and offers intrinsic numerical dissipation due to upwind Riemann fluxes among element interfaces. On the other hand, CG imposes $\mathbf{C}^0$ continuity among mesh elements and, hence, does not possess intrinsic numerical dissipation [5, 6, 7]. This feature is important for numerical convergence of the simulations. In fact, one must add artificial numerical dissipation in order to stabilize simulations that adopt CG, whereas it is not mandatory when using DG. The most common stabilization technique for the CG scheme is the Spectral Vanishing Viscosity (SVV) [8], but recently the Gradient Jump Penalty (GJP) [9] technique has been providing promising results.

To glance the current scenario of the CG and DG, we perform a bibliometric analysis. The selected databases were Web of Science and Scopus. Also, two searches were performed in each database, one for each numerical squeme and all terms used were looked for in the title, abstract and key-words sections of the papers until the year of 2023. The first search combined the string: *"DG" OR "Discontinuous Galerkin"* with the string: *"CFD" OR "Computational Fluid Dynamics" OR "Euler equations" OR "Navier-Stokes equations"* through the boolean operator "AND". The second search looked for: *"CG" OR "Continuous Galerkin"* with *"CFD" OR "Computational Fluid Dynamics" OR "Euler equations" OR "Navier-Stokes equations"* through the boolean operator "AND". The total number of results of each search in Web of Science and Scopus were respectively: 1925, 2420, 194 and 295. One can see that there are many more papers with the DG framework than with CG. Figure 1 presents the time evolution of the published papers in the selected databases, which total sums equal the numbers previous shown. Before 2000, the number of published papers regarding DG is not very different from the published papers with CG. However, a few years later, the number of published papers about DG increased a lot, whereas the number of CG papers increased with a low slope.The previous data show us that SEM have been receiving more attention for the last years, specially the DG scheme. The main reasons for the increasing adoption of those high-order methods may be the ones previous presented as the description of the numerical methods' features, improving numerical performance techniques and accurate results.

In this context of relatively small amount of study about CG and of general knowledge of the SEM advantages, this paper seeks to increase number of analyses regarding the Continuous Galerking formulation within the implict LES approach. To that end, two test cases as simulated here: the Taylor-Green vortex (TGV) and a spatial channel flow (SCF). Both cases adopt the GJP stabilization technique, what have not been done in the literature yet, as far as the authors know. Also, the TGV case is compared with traditional LES results, showing an improved accuracy throughout the flow realization. The SCF is compared with DNS results, showing that the proposed numerical scheme was also able to provide accurate results.

2 Taylor-Green Vortex

The first test case that we work on is the Taylor-Green Vortex. This flow is is an example of a 3D nonlinear flow proposed by Taylor and Green in 1937 [10] to study transition and turbulence, specially the formation of small eddies and their dissipation. The temporal evolution of the TGV is composed by an initial laminar flow, which is unstable to small perturbations, followed by a transition from laminar to turbulent and then a fully-turbulent state with a nearly isotropic

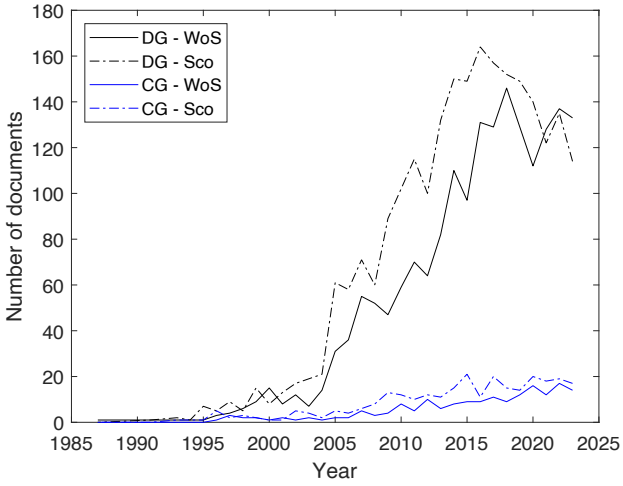

Figure 1: Number of papers published about DG and CG in the Web of Science (WoS) and Scopus (Sco) databases

decay, conducted by vorticity gradients and the vortex-stretching mechanism [11]

The TGV flow is also extensively used to validate new numerical schemes and methods, in particular its compressible version, as many numerical solutions of the flow are available in the literature as references. The flow is also known for numerical divergence, what is usually the case when no extra terms of stabilization are included, even with the DG scheme [12, 13, 14]. Therefore, numerical stabilization techniques are usually employed in TGV simulations in order to add numerical dissipation, thus avoiding divergence. Whereas it is possible to sometimes rely on the intrinsic upwind Riemmann fluxes in the DG scheme, or even apply an artificial dissipation as performed by [3], one has to adopt a numerical stabilization technique as the SVV or GJP for the CG as previous commented. Both have been shown to be successfully in stabilizing simulations, and equivalent as sometimes superior benefits have been found for the GJP [9].

This section analyzes the capability of the CG formulation to solve the incompressible TGV flow, focusing the analysis on the kinetic energy dissipation and energy spectrum. To do so, we simulate the flow with the polynomial order of P = 4 with and without the GJP stabilization technique. Also, the dissipation features and accuracy of the results are compared with classic LES sub-grid models (Smagorinsky and Vreman), two jump penalty strategies (solution and gradient), both coupled with the DG scheme and from [3], and we also compare with DNS results from [15].

2.1 Numerical setup

The Taylor-Green vortex flow is given by the analytical initial conditions of Eq. (3), which is used in incompressible simulations of TGV. Even though the w-velocity component is equal to zero, the developing flow field becomes three-dimensional. The reference parameters are $V_o = L = 1$, where V_o is the initial velocity and L is the integral length scale, and the Reynolds number (Re) is defined as $Re = V_o L/\nu_o$ - where ν is the kinematic viscosity - and is set here to

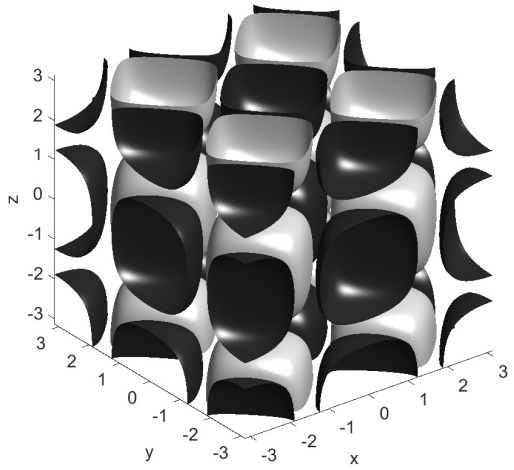

Figure 2: Iso-surfaces of Q-Criterion at the initial condition. Dark (Q = -0.1) and light (Q = 0.1)

1600, which is a common Re analyzed in the literature (see e.g. [3, 16, 17]). Finally, the domain (Ω_{TGV}) is a cube of size $[-\pi L, \pi L]^3$ constituting a basic unit of TGV cells, with triply-periodic boundaries and the simulation is run until a physical time of $14\,L/V_0$. The non-dimensional time-step, $d\tau = dtV_o/L$, adopted for the simulations ranged from 5×10^{-5} to 5×10^{-4}.

$$u = V_o \sin(x/L)\cos(y/L)\cos(z/L) \tag{1}$$

$$v = -V_o \cos(x/L)\sin(y/L)\cos(z/L) \tag{2}$$

$$w = 0$$

The domain is discretized with a mesh of 32^3 elements to match the number of elements used in [3]. As previously cited, the polynomial basis order is P = 4 to match the total number of degrees of freedom (N_{dof}) of the reference. They adopted the DG squeme with a polynomial order P = 3, so we adopt one order higher because of the shared degree of freedom at elements interfaces in CG. The estimated N_{dof} is 2097152 as $N_{dof} = N_{el}P^3$ for the CG scheme. Also, the flow is simulated with and without the stabilization method GJP, P4y and P4n cases respectively, to analyze its influence. Figure 2 pictures the initial condition in terms of iso-surfaces of Q-Criterion. This initial state naturally leads to a symmetry breakdown due to vorticity gradient and vortex-stretching.

2.2 Results and Discussion

Kou et al. [3] studied the TGV flow for the same Re in a compressible flow with Mach number of 0.1. Also, their solver uses the DG scheme, but we have considered these differences as negligible for the comparisons that we make herein. Also, there are many more studies about TGV with compressible flows than incompressible in the literature, what makes a comparison under all the same parameters less likely. The authors investigated the effects of two penalization methods on the accuracy of the solution and the stabilization of the flow. Furthermore, two standard sub-grid models were tested in a LES approach. They obtained stabilized and accurate

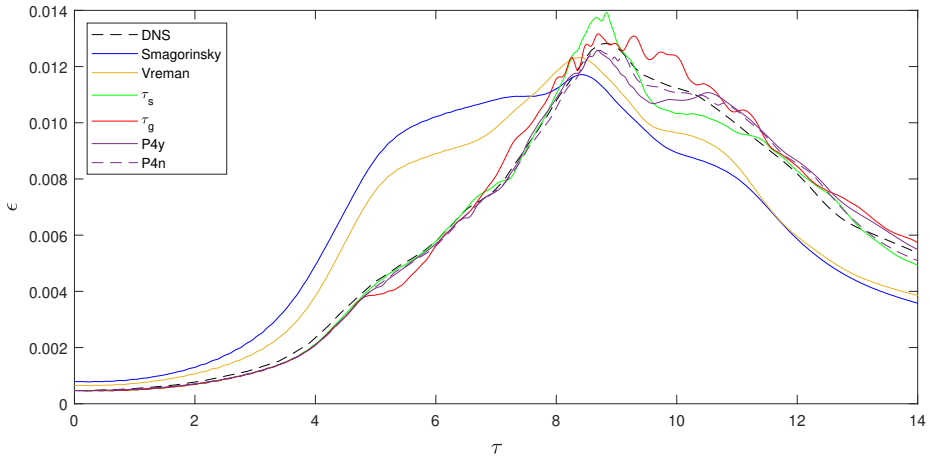

Figure 3: Temporal evolution of kinetic energy dissipation rate and results from [3] and [15]

results with the stabilization methods. The results were also better than the standard sub-grid models.

Figure 3 shows the temporal evolution of the kinetic energy dissipation rate of our simulated cases and the results from [3, 15]. The first thing we note is that our results approach to the DNS case and also to the curves simulated with the penalization methods in DG. Our results are smoother, presenting less oscillations surrounding the kinetic energy dissipation peak, specially when comparing with the penalization based on the gradient jump proposed by the reference. Also, the present results do not over dissipate the flow at and around the peak as happens with the DG scheme. They follow the DNS curve more closely, although the P4y case dissipates less than it should after $\tau \approx 8.5$ until $\tau \approx 11$. As noted by [3], the classic LES closure models supply greater dissipation levels at earlier times ($\tau < 8$), since they already actuate even before the simulation has transitioned to turbulent. So, even though the LES sub-grid models were applied to the DG framework, we can note that the results with the iLES approach with the CG framework provided more accurate result.

Towards evaluating the solution and dissipation effects per length-scale, Fig. 4 presents the 3D kinetic energy spectra of the flow at $\tau = 8$. The spectra is computed with the 3D velocity field using spherical shells of unit width. Although it would be interesting to compare at $\tau = 9$, which is closer to the dissipation peak, all instantaneous kinetic energy dissipation rate values are close to the DNS results at $\tau = 8$, what could mislead to a wrong interpretation that the scales are behaving similarly, which is not the case. Therefore, we can account for an accumulated effect of the wrong dissipation until that time. As exposed by [3], the classic LES closure models greatly dissipate the energy at mid-wavenumbers, consequently they end not capturing a realistic energy level of the smallest length-scales (highest wavenumbers). Again, we observe a similar behavior among the iLES results, mainly until the end of mid-wavenumbers, which allow a more accurate capture of the flow physics. Also, our results at the highest wavenumbers are somewhere between the jump methods' accuracy proposed by the reference.

We finish the TGV analysis with a look on the GJP effects on the solution. The first effect was the stabilization of the simulation. The P4n case required a time-step 10 times smaller than the P4y to not diverge and maintain similar CFL levels. The time-step was decreased during

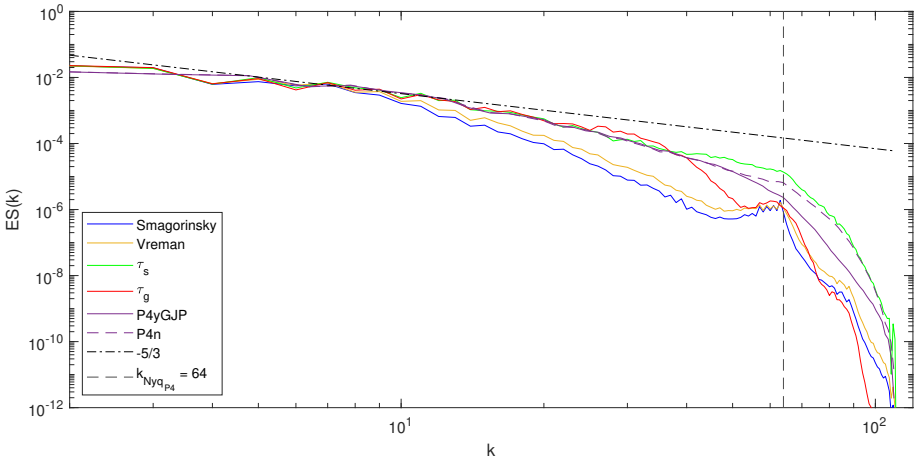

Figure 4: 3D kinetic energy spectra and results from [3]

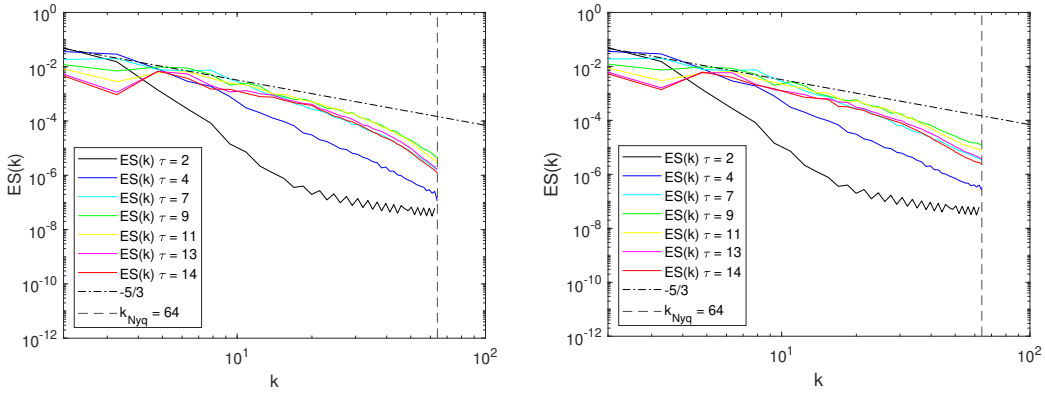

(a) Case P4y (b) Case P4n

Figure 5: Temporal evolution of the 3D kinetic energy spectra

the simulation, what resulted into local small variations of the flow kinetic energy, but also into peaks of the kinetic energy dissipation rate, as the latter is computed with the derivative of the former. Besides the issues with convergence, we can notice the GJP effect on the dissipation of the smallest scales in Fig. 4. After a wavenumber of approximately 50, we see the energy dissipation in the curve of the P4y case when compared with the P4n one. To explore more this effect, Fig. 5 shows the temporal evolution of the 3D kinetic energy spectra. We can see that the flow evolves qualitatively very similar in both cases. What can be directly observed is the effect of the GJP dissipating the energy contained in the smallest scales. This is the expected behavior based on the design of this penalization method [9]. For last, Fig. 6 depicts the differences on the flow solution via iso-contours of non-dimensional Q-criterion for the cases at $\tau = 9$. From them, we can see that the solution with the GJP has a less noisy solution and smoother structures, showing that the penalization method acted dissipating the smallest structures.

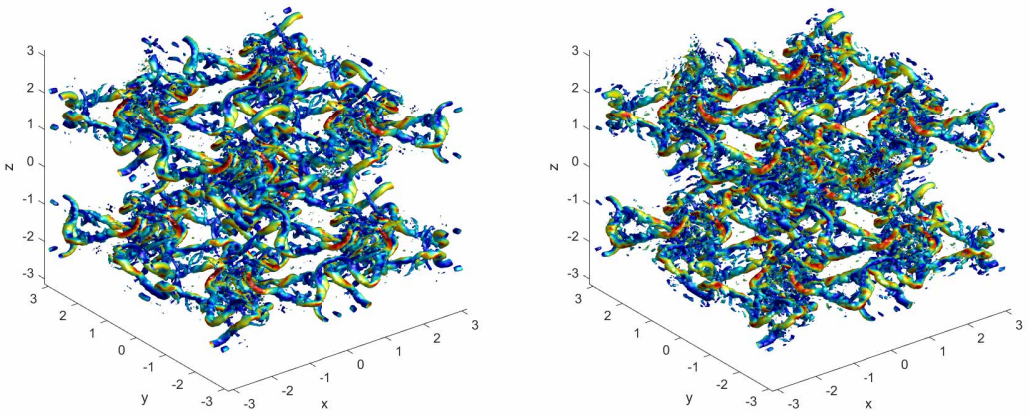

(a) Case P4y (b) Case P4n

Figure 6: Iso-contours of non-dimensional Q-Criterion (Q = 15.0) of both cases at $\tau = 9$. Colored with normalized kinetic energy

3 Spatially evolving turbulent channel flow

We now proceed to our second test case, which is a spatially evolving turbulent channel flow. We draw attention to the fact that this is a spatial simulation not a temporal one. Usually, channel flow simulations adopts a temporal approach (with periodic conditions in the flow direction) instead of a long streamwise distance of the domain, what increases the computational cost. Concerns rise with the adoption of the temporal approach as the domain size could constrain the development of the turbulent flow structures. Also, a temporal case is less similar to real word scenarios, as it would not be able to simulate complex geometries or specific perturbations. This is where a spatial flow simulation can be advantageous or strictly necessary.

A difficulty associated with spatial flows is the space and time necessary for the development of turbulence that may lead to high computational cost. Therefore, one must force the transition to turbulence somehow, specially when dealing with higher fidelity simulations. The imposition of forced fields may be classified in two categories as explained by [18]: mapping (or also called recycling) method and synthetic turbulence method. The former applies a pre-computed flow field and it is re-injected into the inlet of the domain. The latter uses a kind of fluctuation and imposes it into the incoming flow. More details about them can be found in [18] and examples of the applications in [19].

Another reason for the importance of simulating spatially evolving flows using spectral/hp element methods is that the dispersion and diffusion errors differ from periodic to inflow- and outflow-type boundary conditions as shown in [2, 6, 7, 8]. So these differences may require different considerations about the numerical setup as well as differences in the results.

The channel flow is given by a flow bounded by the lower, upper and lateral sides, but the width of the channel is such that the flow statistics become independent in the z direction as long as it is far away from the lateral walls. Also, if we select a position far away from the inlet,

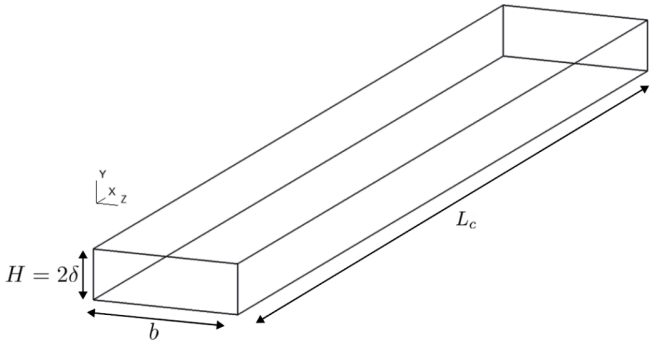

Figure 7: Domain of the channel flow

the flow becomes fully developed and its statistics are symmetric about the central plane and also one-dimensional, varying only with the y direction.

Given that general description, this section analyzes the accuracy of a CG numerical setup on solving a spatially evolving channel flow, focusing the analysis on the capture of the streamwise velocity profile development and on the spatial evolution of the skin friction coefficient. Also, the accuracy is checked comparing the results with DNS data from [20].

3.1 Numerical setup

The planar channel domain is shown in Fig. 7. It has a height of $H = 2\delta = 2$, a width of $b = 6\delta$ and a length of $L_c = 50\delta$, which is a long enough length for the flow to reach a statistically steady regime before the outflow boundary. No-slip boundaries were set to the upper and lower surfaces and periodic boundaries were applied to the lateral surfaces. At the inlet, a velocity profile for the streamwise component was defined by

$$u = \tanh(ay)^c y^{1/b}, \quad 0 \leq y \leq 1 \tag{3}$$

where the constants a, b and c were adjusted to fit the velocity profile of [20], providing a better approximation of the flow in the inner and log layers. Fore more information about this adjustment, the reader is referred to [19].

In order to trigger the transition to turbulence, a body force is applied to a region in the beginning of the domain of a length $L_a = 4$. The forcing term is given by

$$\tilde{f} = \Lambda \sin(\Psi) \tag{4}$$

where Ψ is a random number generated by a Gaussian function with unit variance and zero mean and Λ is a constant equal to 6. The body force act on all velocity components and change each time-step. This procedure has been developed and tested by [21] and [19].

The initial condition was set to a bulk velocity of $u = 1$ and zero to the others components. Also, the kinematic viscosity was chosen as $\nu = 3.5 \times 10^{-4}$ based on the results of [20]. These values results in a Re based on the channel height and bulk velocity of approximately 5714, being equivalent to a $Re_\tau = 182$ according to the reference. Regarding the temporal discretization, the time-step was adjusted to obatin a CFL values less than 0.2.

The simulation is run for 60 convective time units to account for the transient period and then the statistics is gathered for more 90 convective time units for post-processing. These values

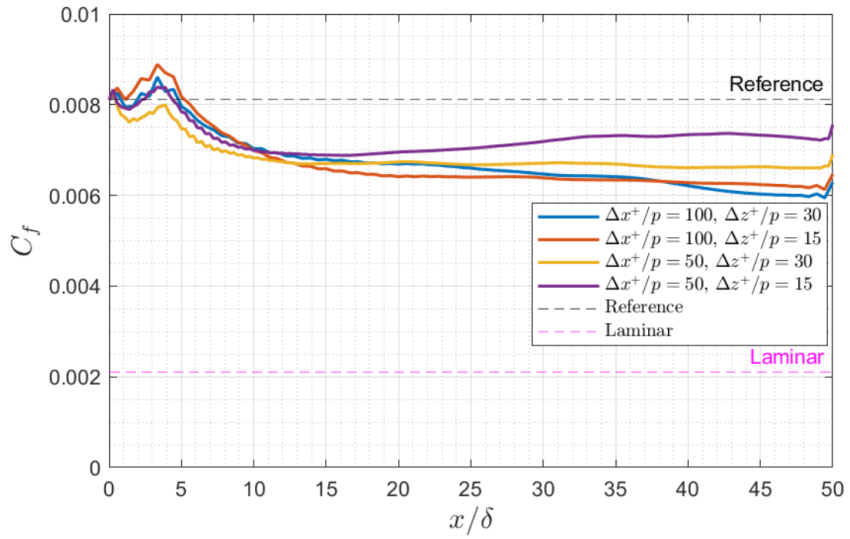

Figure 8: Streamwise evolution of the skin friction coefficient for the different meshes. Reference value from [20]

for the transient and for the statistical convergence were verified to be enough [19]. Finally, the polynomial order adopted for this test case is P = 2.

3.2 Results and Discussion

The grid was not described in the previous section because the accuracy was also analyzed based on a mesh refinement study, so it is presented now. The mesh is constructed with hexahedral structured elements. The elements spacing was kept constant along the streamwise and spanwise directions, whereas a geometric progression was applied to the wall-normal direction to concentrate elements close to the lower and upper surfaces. The general guidelines of [22] were followed, so for a high-order method we have: $50 \leq \frac{\Delta x^+}{p} \leq 150$, $15 \leq \frac{\Delta z^+}{p} \leq 40$ and $\frac{\Delta y^+}{p} < 1$. Then, four meshes were created to investigate the solution sensitivity to the spanwise and streamwise refinement. A fine mesh with $\Delta x^+/p = 50$ and $\Delta z^+/p = 15$, two intermediate ones, one with $\Delta x^+/p = 100$ and $\Delta z^+/p = 15$ and the other with $\Delta x^+/p = 50$ and $\Delta z^+/p = 30$, and a coase mesh with $\Delta x^+/p = 100$ and $\Delta z^+/p = 30$.

Figure 8 shows the streamwise evolution of the skin friction (C_f). One can see that C_f values increase slightly in the beginning due to the perturbed region and suddenly starts to fall after it. Then, all meshes' values tend to converge to values lower than the DNS reference. The closest value is the fine mesh, followed by the one with fine refinement in the streamwise direction. The worst agreement was obtained by the coarse mesh as it would be expected. This show that the C_f is most sensitive to the streawise mesh refinement.

The spatial evolution of the streamwise velocity profile is shown in Fig. 9 for the fine and coarse meshes. The profiles are shown in intervals of 5δ and they were scaled to aid the visualization. In general, the profiles match well the DNS data. The fine mesh keeps a good accuracy throughout the channel, whereas the coarse mesh loses accuracy with the spatial development. This differences in the velocity profiles can be related to the skin friction differences seen in

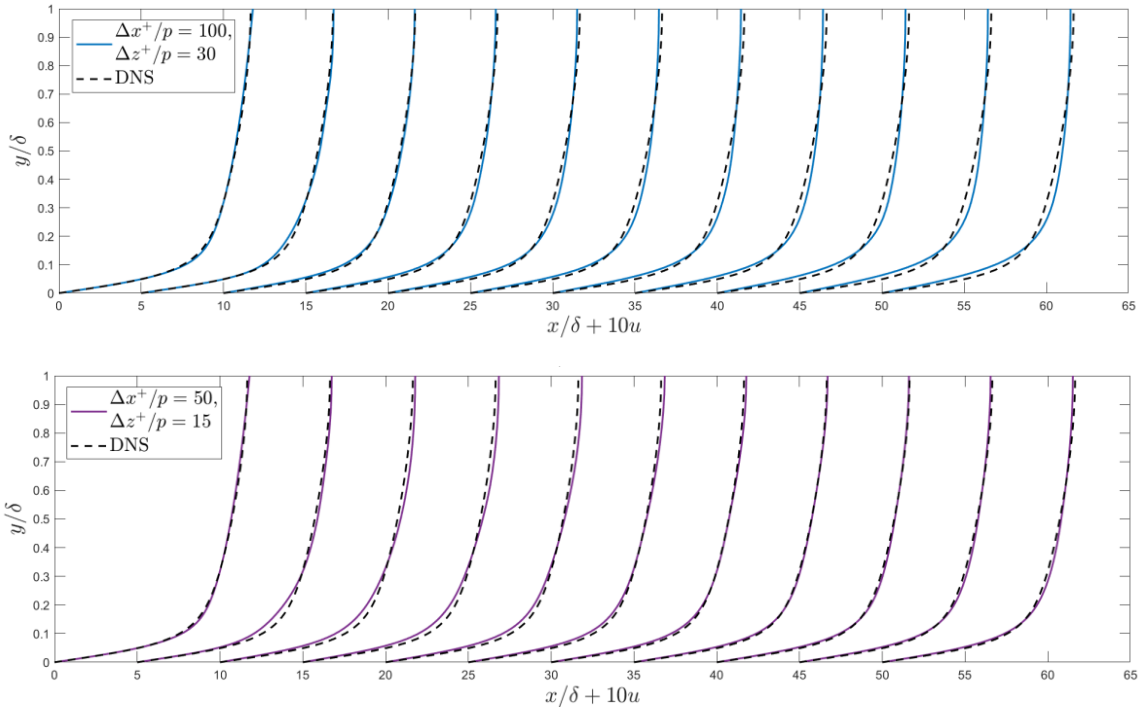

Figure 9: Spatial evolution of the streamwise velocity profiles for the coarse and fine meshes

Fig. 8. So, these results show that the mesh refinement aids to recover the DNS results, as it would be expected, and als that the CG framework with the GJP stabilization is able to provide accurate results of a spatial evolving channel flow.

4 CONCLUSIONS

This paper analyzes two test cases in order to evaluate the accuracy of the high-order Continuous Galerkin scheme within the iLES turbulence approach. The first case, the so-called Taylor-Green vortex, analyzes the transition to turbulence and also turbulence decay. We have been able to see that the CG scheme was able to capture accurate results, specially when compared with traditional LES sub-grid models. Also, the results were comparable with DG ones. Finally, it was also verified the ability of GJP to stabilize the simulations and still provide accurate results.

A spatial developing channel flow was selected as the second test case to verify the CG accuracy in bounded flow with an inlet and outflow boundary conditions. These boundary conditions have been show to possess different dispersion/diffusion properties than the traditional temporal flow approach. The results show that even a coarse wall-resolved mesh is capable of providing accurate results when compared to DNS.

With that, we have obtained results that show the feasibility of the CG scheme to solved transitional and turbulent flows in temporal and spatial approaches. Also, the required use of a stabilization technique, in the present case the GJP, was able to provide stabilization while did not considerably jeopardize the solution.

REFERENCES

[1] POPE, S. B. 2000. Turbulent Flows. New York: Cambridge University Press.

[2] MOURA, R.; SHERWIN, S.; PEIRÓ, J. 2016. "Eigensolution analysis of spectral/hp continuous galerkin approximations to advection-diffusion problems: Insights into spectral vanishing viscosity." Journal of Computational Physics, v. 307, p. 401–422 Available at: https://doi.org/10.1016/j.jcp.2015.12.009.

[3] KOU, J.; MARINO, O. A.; FERRER, E. 2023. "Jump penalty stabilization techniques for under-resolved turbulence in discontinuous galerkin schemes." Journal of Computational Physics, v. 491, p. 112399. Available at: https://doi.org/10.1016/j.jcp.2023.112399.

[4] SLAUGHTER, J.; MOXEY, D.; SHERWIN, S. 2023. "Large eddy simulation of an inverted multi-element wing in ground effect." Flow, Turbulence and Combustion, v. 110, n. 23, p. 917–944. Available at: https://doi.org/10.1007/s10494-023-00404-7.

[5] KARNIADAKIS, G.; SHERWIN, S. J. 2005. Spectral/hp element methods for computational fluid dynamics. 2nd. ed. New York: Oxford University Press.

[6] MOURA, R.; SHERWIN, S.; PEIRO, J. 2015. "Linear dispersion–diffusion analysis and its application to under-resolved turbulence simulations using discontinuous galerkin spectral/hp methods." Journal of Computational Physics, v. 298, p. 695–710. Available at: https://doi.org/10.1016/j.jcp.2015.06.020.

[7] MENGALDO, G.; MOURA, R.; GIRALDA, B.; PEIRO, J.; SHERWIN, S. 2018. "Spatial eigensolution analysis of discontinuous galerkin schemes with practical insights for under-resolved computations and implicit LES." Computers & Fluids, v. 169, p. 349–364, recent progress in nonlinear numerical methods for time-dependent flow & transport problems. Available at: https://doi.org/10.1016/j.compfluid.2017.09.016.

[8] MOURA, R. C.; AMAN, M.; PEIRO, J.; SHERWIN, S. J. 2020. "Spatial eigenanalysis of spectral/hp continuous galerkin schemes and their stabilisation via DG-mimicking spectral vanishing viscosity for high reynolds number flows." Journal of Computational Physics, v. 406, p. 109112. Available at: https://doi.org/10.1016/j.jcp.2019.109112.

[9] MOURA, R. C.; CASSINELLI, A.; DA SILVA, A. F.; BURMAN, E.; SHERWIN, S. J. 2022. "Gradient jump penalty stabilisation of spectral/hp element discretisation for under-resolved turbulence simulations." Computer Methods in Applied Mechanics and Engineering, v. 388, p. 114200. Available at: https://doi.org/10.1016/j.cma.2021.114200.

[10] TAYLOR, G. I.; GREEN, A. E. 1937. "Mechanism of the production of small eddies from large ones." Proceedings of the Royal Society of London. Series A - Mathematical and Physical Sciences, v. 158, n. 895, p. 499–521. Available at: https://royalsocietypublishing.org/doi/abs/10.1098/rspa.1937.0036

[11] SHARMA, N.; SENGUPTA, T. K. 2019. "Vorticity dynamics of the three-dimensional taylor-green vortex problem." Physics of Fluids, v. 31, n. 3, p. 035106, 2019. Available at: https://doi.org/10.1063/1.5083870.

[12] MOURA, R.; MENGALDO, G.; PEIRO, J.; SHERWIN, S. 2017. "On the eddy-resolving capability of high-order discontinuous galerkin approaches to implicit LES/under-resolved DNS of euler turbulence." Journal of Computational Physics, v. 330, p. 615–623. Available at: https://doi.org/10.1016/j.jcp.2016.10.056.

[13] GASSNER, G. J.; WINTERS, A. R.; HINDENLANG, F. J.; KOPRIVA, D. A. 2018. "The BR1 scheme is stable for the compressible navier–stokes equations." Journal of Scientific Computing, v. 77, p. 154–200. Available at: https://doi.org/10.1007/s10915-018-0702-1.

[14] ROJAS, D.; BOUKHARFANE, R.; DALCIN, L.; DEL REY FERNANDEZ, D. C.; RANOCHA, H.; KEYES, D. E.; PARSANI, M. 2021. "On the robustness and performance of entropy stable collocated discontinuous galerkin methods." Journal of Computational Physics, v. 426, p. 109891. Available at: https://doi.org/10.1016/j.jcp.2020.109891.

[15] WANG, Z.; FIDKOWSKI, K.; ABGRALL, R.; BASSI, F.; CARAENI, D.; CARY, A.; DECONINCK, H.; HARTMANN, R.; HILLEWAERT, K.; HUYNH, H.; KROLL, N.; MAY, G.; PERSSON, P.-O. 2013. "High-order CFD methods: current status and perspective." International Journal for Numerical Methods in Fluids, v. 72, n. 8, p. 811–845. Available at: https://onlinelibrary.wiley.com/doi/abs/10.1002/fld.3767.

[16] BRACHET, M. E. 1991. "Direct simulation of three-dimensional turbulence in the taylor–green vortex." Fluid Dynamics Research, v. 8, n. 1-4, p. 1. Available at: https://dx.doi.org/10.1016/0169-5983(91)90026-F.

[17] TONG, G. G.; KAMENSKY, D.; EVANS, J. A. 2022. "Skeleton-stabilized divergence-conforming b-spline discretizations for incompressible flow problems of high reynolds number." Computers & Fluids, v. 248, p. 105667. Available at: https://doi.org/10.1016/j.compfluid.2022.105667.

[18] VEDOVOTO, J. M.; NETO, A. da S.; SILVA, L. F. Figueira da; MURA, A. 2015. "Influence of synthetic inlet turbulence on the prediction of low mach number flows." Computers and Fluids, Elsevier Ltd, v. 106, p. 135 - 153.

[19] PERUCHI ZANCA, A. H. 2023. Simulation of spatially developing turbulent channel flow with spectral/hp element methods. 110 p. Final paper (Undergraduation study) - Instituto Tecnológico de Aeronáutica, São José dos Campos.

[20] MYOUNGKYU, L.; MOSER, R. D. 2015. "Direct numerical simulation of turbulent channel flow up to $Re_{tau} = 520$", Journal of Fluid Mechanics. vol. 774, pp. 395-415. https://doi.org/10.1017/jfm.2015.268

[21] NABAK ROCHA, M. 2022. A simpler approach to generate turbulent boundary layers for eddy-resolving simulations. 100 p. Dissertation Master of Science - Instituto Tecnológico de Aeronáutica, São José dos Campos.

[22] GEORGIADIS, N. J.; RIZZETTA, D. P.; FUREBY, C. 2010. "Large-eddy simulation: Current capabilities, recommended practices, and future research." AIAA Journal, v. 48, n. 8, p. 1772-1784.